Acta Pharmaceutica Sinica B 2026;16(5):3043−3058

Chinese Pharmaceutical Association
Institute of Materia Medica, Chinese Academy of Medical Sciences

Acta Pharmaceutica Sinica B

www.elsevier.com/locate/apsb
www.sciencedirect.com

ORIGINAL ARTICLE

Agonist-specific FPR1 conformational change prevents receptor recycling and promotes targeted protein degradation

Junlin Wang[a,b,*], Qiwen Liao[b,c], Geng Chen[b,d], Yixin Chang[b], Hong Nie[a], Jiahong Lu[e,f], Richard D. Ye[b,g,*]

[a]*State Key Laboratory of Bioactive Molecules and Druggability Assessment, Guangdong Basic Research Center of Excellence for Natural Bioactive Molecules and Discovery of Innovative Drugs/Guangdong Province Key Laboratory of Pharmacodynamic Constituents of TCM and New Drugs Research/International Cooperative Laboratory of Traditional Chinese Medicine Modernization and Innovative Drug Development of Ministry of Education (MOE) of China, College of Pharmacy, Jinan University, Guangzhou 510632, China*
[b]*Kobilka Institute of Innovative Drug Discovery, School of Medicine, The Chinese University of Hong Kong, Shenzhen 518172, China*
[c]*Department of Food Science and Nutrition, The Hong Kong Polytechnic University, Kowloon, Hong Kong SAR 999077, China*
[d]*School of Medicine, Shenzhen Campus of Sun Yat-sen University, Sun Yat-sen University, Shenzhen 518107, China*
[e]*State Key Laboratory of Mechanism and Quality of Chinese Medicine, Institute of Chinese Medical Sciences, University of Macau, Macau SAR 999078, China*
[f]*Guangdong-Hong Kong-Macau Joint Lab on Chinese Medicine and Immune Disease Research, University of Macau, Macau SAR 999078, China*
[g]*The Chinese University of Hong Kong, Shenzhen Futian Biomedical Innovation R&D Center, Shenzhen 518048, China*

Received 24 May 2025; received in revised form 17 August 2025; accepted 10 October 2025

KEY WORDS

G protein-coupled receptors;
Cryo-EM;
Formyl peptide receptors;
Receptor recycling;

Abstract Recycling of internalized cell surface receptors is critical for membrane transport and receptor-mediated signaling. Formyl peptide receptor 1 (FPR1) plays important roles in host defense and inflammatory tissue injury. Here we report that fMet-Leu-Phe-Cys (fMLFC), a peptide agonist of FPR1, prevents recycling of internalized FPR1 and diverts it to the late endosome and lysosome for degradation. In contrast, FPR1 bound to the classic ligand fMLF interacts with RAB11 and SNX17, facilitating its recycling back to the cell surface. We determined a cryo-EM structure of fMLFC-bound FPR1

*Corresponding authors.
E-mail addresses: wangjunlin@jnu.edu.cn (Junlin Wang), richardye@cuhk.edu.cn (Richard D. Ye).

Peer review under the responsibility of Chinese Pharmaceutical Association and Institute of Materia Medica, Chinese Academy of Medical Sciences.

https://doi.org/10.1016/j.apsb.2026.03.019

Protein degradation;
Acute lung injury;
Sorting nexins;
Small GTPases

−Gi complex. Alanine substitutions of key residues that interact with fMLFC (F102A, T177A, F178A) improved FPR1 recycling. Using a FlAsH−NanoBRET-based FPR1 biosensor, the fMLFC-induced receptor conformational change was found to be different from the fMLF-induced conformational change. fMLFC stimulation reduced FPR1 cell surface expression, along with reduced acute lung injury in LPS-treated mice. Our findings suggest that fMLFC is a chemical knockdown agent that promotes targeted protein degradation and reduces FPR1-mediated inflammation.

1. Introduction

G protein-coupled receptors (GPCRs), also known as seven transmembrane receptors, are primarily located on the cell surface to sense extracellular signals. When stimulated by an agonist, changes in receptor conformation lead to the activation of various intracellular signaling proteins, including heterotrimeric G proteins, G protein-coupled receptor kinases (GRKs), and β-arrestins, thereby triggering distinct downstream signaling cascades[1-4]. Ligand-bound receptor internalization is a broadly existing cellular phenomenon. Most internalized GPCRs enter recycling vesicles and return to the cell surface for a new cycle of activation[5-7]. The RAB proteins are small GTPases that localize to specific intracellular compartments and orchestrate receptor internalization and recycling[8,9]. For example, RAB4 and RAB11 are located in recycling endosomes for the regulation of receptor recycling[10-14]. RAB5 localizes to early endosomes and serves as a marker for the early endosome. RAB7 is found in late endosomes. Furthermore, additional proteins known as sorting nexins (SNXs) are implicated in the recycling pathway[15]. Within this group of SNXs, SNX3 and SNX17 have been reported to play pivotal roles in regulating the recycling behavior of proteins[16-18]. Another route leads the internalized receptor to lysosomal degradation[19-24]. Lysosomes are acidic compartments capable of degrading intracellular proteins[25,26]. The internalized receptor enters the early endosomes, then transfers to the late endosomes that fuse with lysosomes for protein degradation.

Various genetic approaches exist for downregulating the expression level of target proteins, including small interfering RNA (siRNA), short hairpin RNA (shRNA) and microRNA (miRNA). However, these technologies still face challenges in terms of improving their selectivity, stability, and safety profiles[27,28]. In order to address these limitations, chemical knockdown methods are employed for protein downregulation. Small molecules[29-31] or intracellular antibodies (intrabodies)[32,33] specifically designed to target certain proteins offer potential solutions to overcome the challenges associated with genetic knockdown technologies. The majority of small molecule-based knockdown strategies use proteolysis-targeting chimera (PROTAC) technology[34,35]. An intrabody, defined as an antibody fragment, exhibits the capacity to bind to a specific target protein and subsequently inhibits its functional activity. Intrabodies are categorized into 2 distinct types: cytosolic intrabodies and endoplasmic reticulum (ER)-retained intrabodies. In the context of intrabody technology, a vector harboring the cDNA encoding the intrabody is transfected into cells to facilitate the expression of the intrabody, thereby enabling inhibition of functions of the target protein. For ER intrabodies[19,36], an ER retention sequence (KDEL) is fused to the C-terminus of the intrabody, effectively preventing its secretion along with the bound target protein.

Formyl peptide receptor 1 (FPR1), a member of class A GPCRs, is predominantly localized on the plasma membrane of neutrophils but also found in lower abundance in other cells, including endothelial and epithelial cells. FPR1 exhibits significant involvement in a multitude of diseases, including lung injury, inflammation, glioblastoma, and breast cancer[37-39]. Various approaches have been devised for the characterization of FPR1[40-42]. FPR1 recognized N-formylated peptides produced in bacteria or mitochondria as a molecular pattern. Among these formyl peptides, fMet-Leu-Phe (fMLF) is the first characterized and most often used peptide originating from *E. coli* with full agonistic activities[43]. Upon activation by fMLF, FPR1 triggers various biological activities such as calcium flux, superoxide generation, and cell migration[43]. FPR1 also internalizes into cells and recycles to the cell membrane for another round of activation. Although FPR1 internalization has long been observed[44], its recycling mechanism remains unclear. In a previous study, we found that a cystine-modified formyl peptide, fMet-Leu-Phe-Cys (fMLFC), exhibited properties different from those of fMLF, such as higher potency in both the Ca^{2+} mobilization assay and the competitive binding assay[45]. In the present study, Cryo-EM (for solving the fMLFC−FPR1−Gi complex structure) and FPR1 biosensor (for FPR1 conformational change) were used together with confocal imaging of proteins involved in receptor trafficking to investigate the mechanism of fMLFC-induced loss of cell surface FPR1. Our results showed that fMLFC can be used as a cell surface FPR1 knockdown agent to abrogate transmembrane signaling and alleviate acute lung injury in a mouse model. fMLFC, therefore, has potential for further development as a therapeutic for inflammatory diseases.

2. Methods and methods

2.1. Materials

fMLFC and fMLFIIK−FITC were synthesized at ChinaPeptides, Shanghai, China. The siRNAs targeting SNX3 and SNX17 utilized in this study were obtained from RiboBio, located in Guangzhou, China. Alexa Fluor 647-labeled mouse anti-human fMLP receptor (Clone 5F1, RUO) was obtained from BD Biosciences, San Jose, CA, USA. fMLF, chloroquine (CQ), 1,2-ethanedithiol (EDT), horseradish peroxidase (HRP), isoluminol (ISO), cytochalasin B, hexadecyltrimethylammonium bromide (CTAB), 3,3′,5,5′-tetramethylbenzidine, and 4-nitrophenyl *N*-acetyl-β-D-glucosaminide were obtained from Sigma−Aldrich, St.

Louis, MO, USA. FLIPR calcium 5 reagent was purchased from Molecular Devices, San Jose, CA, USA. Coelenterazine H was purchased from Promega, Madison, WI, USA. TC-FlAsH II In-Cell Tetracysteine Tag Detection Kit was purchased from Invitrogen, Carlsbad, CA, USA.

2.2. Cell culture

HeLa cells (ATCC, CCL-2) were grown in DMEM containing 10% fetal bovine serum (FBS) and 1% PS. FPR1 stable expressed RBL-2H3 cells (RBL FPR1, ATCC CRL-2256) were maintained in DMEM supplemented with 20% FBS and 250 μg/mL G418. HL-60 cells (ATCC CCL-240) were grown in RPMI 1640 medium containing 20% FBS, 1% PS. For differentiation, HL-60 cells were maintained in HL-60 culture medium containing 1.3% DMSO at a density of 5×10^5 cells/mL and cultured for 5 days to achieve differentiated HL-60 (dHL-60). The differentiation medium was changed every other day.

2.3. Plasmid construction

The plasmids containing complete coding sequences of human RAB4 S22N, RAB4, RAB11 S25N, and RAB11 were generously provided by Professor Guangpu Li (University of Oklahoma Health Sciences Center, USA). pcDNA3.1 mRuby2 and pcDNA3.1 Clover were from Invitrogen (Carlsbad, CA, USA). Plasmid containing the complete coding sequences of Nanoluc was acquired from Promega, Madison, WI, USA. The FPR1 biosensor, utilizing FlAsH NanoBRET technology, was designed to incorporate the tetracysteine tag (amino acid sequence: CCPGCC) into three distinct intracellular loops (ICLs) of FPR1 (FPR1-FlAsH-ICL1-NanoLuc: between amino acid residues T56 and H57. FPR1−FlAsH−ICL1−NanoLuc: between amino acid residues T133 and Q134. FPR1-FlAsH-ICL1-NanoLuc: between amino acid residues L233 and I234) by overlap PCR, and then the C terminus of FPR1 containing the CCPGCC tag was fused with Nanoluc. cDNA of RAB7, RAB4 S22N, RAB4, RAB5, RAB11 S25N, RAB11, SNX17, SNX3, and Clover were subcloned into the PCDNA3.1 plasmid. Clover linked to the N-terminal of the target protein and formed Clover RAB7, Clover RAB4 S22N, Clover RAB4, Clover RAB5, Clover RAB11 S25N, Clover RAB11, Clover SNX17, Clover SNX3. The cDNA of FPR1 was subcloned into the pcDNA3.1 Clover and pcDNA3.1 mRuby2 vectors, resulting in 2 constructs, FPR1-mRuby2 and FPR1-Clover, respectively. All plasmids were verified by DNA sequencing.

2.4. Transfection with plasmid and siRNA

HeLa cells were transfected or co-transfected with different plasmids using Lipofectamine 3000 (Invitrogen) according to the reagent protocol when cells were grown to 80% confluency. The transfection efficiency was about 70%. Then cells were incubated at 37 °C with 5% CO_2 for 24 h for different assays. For transfection of different kinds of siRNA (Target SNX3[46]: 5′-AACAAGGGCUGGAGCAGUUUAdTdT-3′, Target SNX17[47]: 5′-CUGGCUUUUGAAUACCUCAdTdT-3′), HeLa cells were cultured to 40% confluency and then transfected with Lipofectamine 3000 without using P3000 reagent during the siRNA dilution step. The final concentration of siRNA in the cell culture medium was adjusted to 50 nmol/L. The cells were cultured at 37 °C with 5% CO_2 for 48 h. Subsequently, the cells were transfected with FPR1−GFP and further incubated at 37 °C with 5% CO_2 for an additional 24 h before conducting various assays.

2.5. qPCR analysis

The HeLa FPR1-GFP cells that were transfected with siRNA were lysed by the TRIzol Reagent (Thermo Fisher Scientific, Waltham, MA, USA) to extract total RNA. 500 ng RNA was used for cDNA synthesis using PrimeScript RT Master Mix (Takara Bio, Otsu, Japan). The cDNA, Sequence-specific primers (SNX17 forward primer: 5′-GGTCAACGTGCTAACTTCAGA-3′, SNX17reverse primer: 5′-GCTCCATCCTCTTTTTCTCGAAC-3′; β-actin forward primer: 5′-AGAGCTACGAGCTGCCTGAC-3′, β-actin reverse primer: 5′-AGCACTGTGTTGGCGTACAG-3′; SNX3 forward primer: 5′-CCAAGCCGCAGAACCTGAAT-3′, SNX3 reverse primer: 5′-GACCCTGATTTCGTAAGTGGTG-3′) and SYBR premix Ex taq II (Takara Bio) were used for mRNA level detection using ViiA 7 Real-Time PCR System (Thermo Fisher Scientific).

2.6. Flow cytometry

For FPR1 recycling assay, HeLa FPR1-GFP cells (transient transfected with FPR1-GFP), dHL-60 cells, RBL FPR1 cells, RAW264.7 cells or HeLa cells co-transfected with FPR1 mRuby2 and RAB plasmid (Clover RAB4 S22N, Clover RAB4 WT, Clover RAB11 S25N, Clover RAB11 WT) or HeLa FPR1-GFP transfected with different siRNA (si Negative control (siNC), si*SNX17* and si*SNX3*) were harvested, washed with PBS and resuspended in the culture medium. fMLFC (5 μmol/L) or fMLF (5 μmol/L) were added to the medium and incubated for 1 h at 37 °C to induce FPR1 internalization. To quantify membrane FPR1, 2 distinct fluorescent probes were used: A human-specific anti-FPR1 antibody (Alexa Fluor 647 Mouse Anti-Human fMLP receptor) for the detection of human FPR1, and an FITC-labelled peptide (fMLFIIK−FITC) that binds to mouse FPR1 (FPR1). After incubation, FPR1 or FPR1-bound fluorescence was measured by flow cytometry. Total FPR1 (membrane plus cytoplasmic) was assessed by constitutively expressing a GFP-tagged FPR1 construct and recording global GFP fluorescence signal by flow cytometry. For measurement of receptor cycling, the cells were transferred to ice and washed 3 times with PBS. Subsequently, the cells were resuspended in prewarmed cell culture medium and incubated for 1 h at 37 °C to allow the receptor to be recycled. The receptor on the cell membrane was labeled by fMLFIIK−FITC or FPR1 antibody (Alexa Fluor 647 Mouse Anti-Human fMLP receptor). The receptors on the cell surface were quantified by flow cytometry (BD Accuri C6, BD Biosciences). Quantification of cell surface FPR1 was conducted by setting unstimulated cells as 100%, and the receptor quantity of treatment groups was calculated as a percentage of the control group, as Eq. (1):

$$\text{Cell surface FPR1 (\%)} = (\text{The receptor number of the treatment group/The receptor number of the control group}) \times 100 \quad (1)$$

For the calculation of the absolute number of cells or molecules bound, the specific activity of the labeled ligand or antibody is known, and collected data is compared with BD CellView calibration beads, which enables automated calibration of the flow cytometer.

For FPR1 degradation assay, HeLa FPR1-GFP cells were pre-incubated for 1 h and kept in the presence of 1 μmol/L cycloheximide (CHX, YEASEN, Shanghai, China) then the cells were treated with lysosomal inhibitor chloroquine (CQ, 30 μmol/L), MG 132 (100 nmol/L) and bafilomycin A1 (BAF, 100 nmol/L) for 9 h at 37 °C in the presence of 5 μmol/L fMLFC. Then the cells were washed with PBS. The total number of FPR1 was detected with the green fluorescence intensity of GFP by flow cytometry.

2.7. Confocal microscopy

For the FPR1 recycling assay, HeLa cells were seeded onto glass coverslip in a 24-well plate, co-transfected with RAB plasmid and FPR1 mRuby2, and incubated for 24 h, or transfected with siRNA and FPR1-GFP as described above. The cells were then treated with 5 μmol/L fMLFC or fMLF for 1 h at 37 °C to induce FPR1 internalization. The cells were washed with PBS for 2 times to remove fMLFC and fMLF and incubated with complete medium for 1 h to allow the FPR1 to recycle to the cell membrane. The cells were then washed with PBS and fixed with 4% paraformaldehyde (PFA) at room temperature for 10 min. The siRNA-treated cells were stained with 2 μg/mL Hoechst for 10 min at room temperature and detected by confocal microscopy (LEICA TCS SP8).

For the FPR1 degradation assay. HeLa cells were co-transfected with FPR1 and Clover RAB7, Clover RAB5, and mCherry LAMP1 for 24 h at 37 °C. The cells were treated with 5 μmol/L fMLF or fMLFC for 9 h at 37 °C. Then cells were visualized by confocal microscopy as described above. The images were taken with a 40 × oil objective. The excitation wavelength of GFP and Clover was 488 nm, and the emission wavelength was 500−525 nm. The excitation wavelength of Hoechst was 405 nm, and the emission wavelength was 410−490 nm. For mRuby2 and mCherry, the excitation wavelength was 552 nm, and the emission wavelength was 565−650 nm. Colocalization level of FPR1 and SNX protein or RAB protein was estimated using the function of Image J Plugins (colocalization finder). For each data point, 3 fixed areas of the same size were chosen from the image of interest, and light density was determined using red and green channels, respectively. Pearson's correlation coefficient (*R*r) was then calculated and plotted.

2.8. FlAsH NanoBRET-based biosensor assay

This assay utilized bioluminescence resonance energy transfer (BRET) technology. HeLa cells were transfected with FlAsH NanoBRET-based FPR1 biosensor (FPR1-FlAsH-ICL1-Nanoluc, FPR1-FlAsH-ICL2-Nanoluc or FPR1-FlAsH-ICL3-Nanoluc) for 24 h at 37 °C. The cells were stained with FlAsH-EDT_2 at a concentration of 1 μmol/L containing 2 μmol/L 1,2-ethanedithiol (EDT) for 1 h at 37 °C. Then, wells were washed with PBS 3 times. The cells were seeded in the 96-well white opaque plate at a density of 1×10^5 cells/well, after which the cells were incubated with 5 μmol/L Coelenterazine H for 5 min at 37 °C. The BRET ratio was recorded after stimulation with 5 μmol/L fMLF or fMLFC by the envision plate reader (PerkinElmer Life Sciences, Hopkinton, MA, USA). The BRET ratio was defined by Eq. (2):

$$\text{BRET ratio} = \text{Emission 515 nm/ Emission 460 nm.} \quad (2)$$

2.9. BRET assay

For the Nanoluc Venus BRET system, HEK 293T Cells were seeded in a 24-well plate, co-transfected with FPR1-Nanoluc plasmid and Venus-RAB 11 plasmid (ratio of 1:3), and incubated for 24 h. Then the cells were harvested and resuspended in the culture medium. fMLFC (5 μmol/L) or fMLF (5 μmol/L) were added to the medium and incubated for 1 h at 37 °C to induce FPR1 internalization. Subsequently, the cells were resuspended in prewarmed cell culture medium and incubated for 1 h at 37 °C to allow the receptor to be recycled, after which the cells were incubated with 10 μmol/L furimazine for 5 min at 37 °C. The BRET ratio was recorded by an Envision plate reader (PerkinElmer Life Sciences). The BRET ratio was defined by Eq. (3):

$$\text{BRET ratio} = \text{Emission 535 nm/ Emission 460 nm.} \quad (3)$$

For the Nanoluc Halo tag BRET system, HEK 293T Cells were seeded in a 24-well plate, co-transfected with FPR1-Nanoluc plasmid and Halo tag-SNX17 plasmid (ratio of 1:3), and incubated for 24 h at 37 °C. Then the cells were harvested and incubated with 100 nmol/L Halo tag 618 ligand for 16 h at 37 °C. fMLFC (5 μmol/L) or fMLF (5 μmol/L) were added to the medium and incubated for 1 h at 37 °C to induce FPR1 internalization. Subsequently, the cells were resuspended in prewarmed cell culture medium and incubated for 1 h at 37 °C to allow the receptor to be recycled, after which the cells were incubated with 10 μmol/L furimazine for 5 min at 37 °C. The BRET ratio was recorded by the Envision plate reader (PerkinElmer Life Sciences). The BRET ratio was defined by Eq. (4):

$$\text{BRET ratio} = \text{Emission 615 nm/ Emission 460 nm.} \quad (4)$$

For FPR1 FPR2 dimerization, HEK293 cells were transfected with FPR1-EYFP and FPR2-Nanoluc constructs for 24 h at 37 °C. Then cells were treated with 10 μmol/L furimazine for 5 min fMLF (5 μmol/L), fMLFC (5 μmol/L), or PBS were added to the cell solution, and the BRET ratio was recorded. The BRET ratio was defined by Eq. (3).

2.10. Ligand binding

RBL-FPR2 cells were harvested and suspended to 1×10^5 cells/mL in HBSS buffer containing 0.5% BSA. The cell solutions were pre-incubated with 5 μmol/L fMLFC or 100 nmol/L Wpep (WKYMVm) on ice for 30 min, followed by the addition of 200 nmol/L Wpep-FITC (WKYMVm-FITC) for 1 h on ice. Then the cells were washed with 1 mL PBS and resuspended in HBSS buffer, and MFI of FITC was measured by flow cytometry.

2.11. Chemotaxis assay

Cell migration assay was performed using a 24-well chemotaxis chamber (Transwell, pore size 3 μm, Corning, New York, NY, USA). The dHL-60 cells (2×10^6 cells/mL, 100 μL) were suspended in RPMI 1640 medium containing 0.1% BSA and added to the top chambers. fMLF (10 nmol/L) was mixed with different concentrations of fMLFC, then added to the bottom chambers. After incubation for 2 h at 37 °C. The cells that migrated to the bottom chambers were counted by hemocytometer.

2.12. Superoxide generation

dHL-60 cells were harvested by centrifugation and resuspended in HBSS buffer containing 0.5% bovine serum albumin (BSA) at 5×10^5 cells/mL. The dHL-60 cells were incubated with 40 U/mL of horseradish peroxidase (HRP) and 100 μmol/L isoluminol (ISO) for 5 min at 37 °C in the dark. Then, 200 μL aliquots of cell solution were added into the 96-well plate (a white, flat-bottom tissue culture-treated plate) and assayed for chemiluminescence (CL) at 37 °C in an envision multimode plate reader (PerkinElmer Life Sciences). The CL counts per second (cps) were recorded for around 50 s before and 6 min after stimulation with different concentrations of fMLF and fMLFC.

2.13. Protein expression vector design

For protein expression, human FPR1 was constructed into the pFastBac vector for expression. The coding sequence of FPR1 was fused with an N-terminal HA signal peptide followed by a FLAG tag, an HRV 3C protease cleavage site (LEVLFQGP), and the thermostabilized apocytochrome b562 RIL (BRIL) fusion protein. Human dominant negative Gαi1 (DNGαi1), generated by site-directed mutagenesis to incorporate mutations A326S and G203A of Gαi1, was cloned into the pFastBac vector. Gγ2 and N-terminal 6 × His-tagged Gβ1 were cloned into the pFastBac-dual vector. The coding sequence of scFv16 was fused with a GP67 signal peptide at the N-terminus and an 8 × His tag at the C-terminus, and then cloned into the pFastBac vector.

2.14. Expression and purification of the fMLFC−FPR1−Gi−scFv16 complexes

The baculoviruses of FPR1, Gβ1, Gγ2, and DNGαi1 were generated by using the Bac-to-Bac baculovirus expression system in Sf9 cells, as described previously[48]. When the cell density reached 3.5×10^6 cells/mL (total 2.5 L), 3 types of baculoviruses (FPR1, Gβ1γ2, DNGαi1) were co-expressed in Sf9 insect cells at the ratio of 1:2:4 (total volume of baculoviruses: 26 mL). After infection for 60 h, the cells were collected by centrifugation at 2000 × *g* for 15 min and kept frozen at −80 °C for complex purification usage.

For the purification of fMLFC−FPR1−Gi−scFv16 complexes, cell pellets were resuspended in 300 mL lysis buffer (10 mmol/L Tris pH 7.5, 2.5 μg/mL leupeptin and 160 μg/mL benzamidine, 1 mmol/L EDTA, 3 μmol/L fMLFC and 1 mg/mL iodoacetamide) for 30 min at RT. The lysate was spun for 15 min at 18,000 × *g*, and then pellet was homogenized in 200 mL solubilization buffer (20 mmol/L HEPES pH 7.5, 10% glycerol, 100 mmol/L NaCl, 0.1% cholesteryl hemisuccinate (CHS), 1% dodecylmaltoside (DDM), 2.5 μg/mL leupeptin and 160 μg/mL benzamidine, 2 mg scFv16, 25 mU/mL apyrase, 3 μmol/L fMLFC, 1 mg/mL iodoacetamide) using a Dounce homogenizer and a tight pestle. The sample was stirred for 2 h at 4 °C and then spun 30 min at 18,000 × *g* to remove insoluble debris. The solubilized fraction was incubated with 1.7 mL anti-FLAG affinity resin (GenScript Biotech, Piscataway, NJ, USA) and stirred at 4 °C for 2 h. The resin was manually loaded onto a gravity-flow column and washed with FLAG wash buffer (W1: 20 mmol/L HEPES pH 7.5, 0.01% CHS, 0.1% DDM, 2 mmol/L $CaCl_2$, 100 mmol/L NaCl, 3 μmol/L fMLFC. W2: 20 mmol/L HEPES pH 7.5, 0.02% CHS, 0.2% lauryl maltose neopentyl glycol (LMNG), 100 mmol/L NaCl, 3 μmol/L fMLFC, 2 mmol/L $CaCl_2$) by mixing W1 and W2 buffer in the following ratios: 5 mL:5 mL, 2 mL:8 mL, 1 mL:9 mL, 0.5 mL:9.5 mL, 0 mL:10 mL, respectively. The fMLFC−FPR1−Gi−scFv16 complexes were eluted with 10 mL elution buffer (20 mmol/L HEPES pH 7.5, 0.002% CHS, 0.01% LMNG, 100 mmol/L NaCl, 5 mmol/L EDTA,3 μmol/L fMLFC, 0.2 mg/mL FLAG peptide). The eluted complex was concentrated to 400 μL in an Amicon Ultra-15 Centrifugal Filter Unit (Millipore, Burlington, MA, USA) and further purified through a Superose 6 Increase 10/300 GL (GE Healthcare Life Sciences, Marlborough, MA, USA) equipped in an ÄKTA Fast Protein Liquid Chromatography (FPLC) system with running buffer (20 mmol/L HEPES pH 7.5, 0.01% LMNG, 100 mmol/L NaCl, 0.002% CHS, 3 μmol/L fMLFC). Eluted fractions consisting of fMLFC−FPR1−Gi−scFv16 complexes were pooled and concentrated before being flash frozen in liquid nitrogen and stored at −80 °C.

2.15. Expression and purification of scFv16

The antibody fragment scFv16 was purified as a secretory protein[49]. Briefly, *Trichoplusia ni* Hi5 insect cells were cultured to a density of 3.5×10^6 per milliliter (mL) and infected with the virus of scFv16 at a ratio of 1:50. After 60 h, the supernatant was collected and loaded onto a Ni-NTA resin column. The column was further washed with 20 mmol/L HEPES (pH 7.5), 20 mmol/L imidazole, and 500 mmol/L NaCl and then eluted with 20 mmol/L HEPES (pH 7.5), 250 mmol/L imidazole, and 100 mmol/L NaCl. The eluted protein was concentrated and loaded onto a Superose 6 Increase 10/300 GL (GE Healthcare Life Sciences). Finally, the concentrated scFv16 was flash frozen and stored in liquid nitrogen until further use.

2.16. Cryo-electron microscopy (cryo-EM) sample preparation and data collection

For fMLFC−FPR1−Gi−scFv16 complex, amorphous alloy film (CryoMatrix nickel titanium alloy film, Zhenjiang Lehua Electronic Technology Co., Ltd.) was glow-discharged at Tergeo-EM plasma cleaner. 3 μL purified complex sample (5 mg/mL) was applied onto the grid and then blotted for 3 s with blotting force of 0 and quickly plunged into liquid ethane cooled by liquid nitrogen using Vitrobot Mark IV (Thermo Fisher Scientific). Cryo-EM data were collected by a 300 kV Titan Krios Gi3 microscope (Thermo Fisher Scientific). The raw movies were recorded by a Gatan K3 BioQuantum Camera at a magnification of 105,000, and the pixel size is 0.83 Å. Inelastically scattered electrons were excluded by a GIF Quantum energy filter (Gatan, Pleasanton, CA, USA) using a slit width of 20 eV. The movie stacks were acquired with the defocus range of −1.2 to −2.0 μm with a total exposure time of 2.5 s, fragmented into 50 frames (0.05 s/frame). The semi-automatic data acquisition was performed using SerialEM. A total of 3182 image stacks were collected in 30 h.

2.17. Image processing and model building

Data processing was performed using cryoSPARC 3.3.1 (Structura Biotechnology Inc., Toronto, Canada). The image stacks were first subjected to patch motion correction and patch CTF estimation. 2,285,002 particles were auto-picked and then subjected to 2D classification, and 1,250,339 particles were selected for ab initio reconstruction. After 2 rounds of heterogeneous refinements, a

final set of 866,469 particles was subject to non-uniform refinement and local refinement, yielding a map at 3.03 Å.

The coordinates of FPR1, Gi1, and scFv16 from fMLF−FPR1−Gi (PDB ID: 7WVU/7EUO) were used as templates. All models were docked into the EM density map using UCSF Chimera version 1.12, followed by iterative manual building in Coot-0.9.2 and refinement in Phenix-1.18.2. The final model statistics were validated by Phenix-1.18.2. Structure figures were generated by Chimera or PyMOL (Schrödinger, Inc., New York, NY, USA). The data-collection and structure-refinement statistics are shown in Supporting Information Table S1.

2.18. Animals

Male C57BL/6 mice (8 weeks of age, 20−25g) were used for this study. All experiments were approved by the local ethical authorities (see below).

2.19. Mouse model of LPS-induced acute lung injury

Twenty-four male mice (8 weeks of age, 20−25 g) underwent general anesthesia. The mice were intratracheally inoculated with 2 mg/kg LPS for 6 h to induce acute lung injury. The animals were randomly separated into groups to receive fMLFC (4 mg/kg) *via* the tail vein injection 1 h before the induction of lung injury (fMLFC−LPS group). The mice were divided into four groups: sham, fMLFC only (4 mg/kg, tail vein injection), LPS only (intratracheal inoculation), and fMLFC−LPS. Mouse blood was collected by cardiac puncture, and lungs were removed under anesthesia after 6 h. The left lung was fixed in 4% polyoxymethylene for histologic examination. The right lung was used for myeloperoxidase (MPO) activity detection.

2.20. Mouse neutrophil surface FPR1 detection

Mouse blood was collected, and the erythrocytes were removed by hypotonic lysis with red blood cell lysis buffer (Biolegend, Fell, Germany), and the remaining cells were resuspended in PBS. Mouse neutrophils were isolated using Percoll (GE Healthcare Life Science). The Mouse formyl peptide receptor (FPR1) on the neutrophil cell membrane was labeled by 250 nmol/L fMLFIIK−FITC for 1 h on ice. Then the FPR1 on the cell surface was quantified by flow cytometry.

2.21. Myeloperoxidase activity assay

Mouse lungs were homogenized in 0.5 mL PBS. After centrifugation at 13,000×*g* for 30 min at 4 °C, the pellet was resuspended in 1 mL PBS containing 0.5% hexadecyltrimethylammonium bromide (CTAB) and treated with 2 cycles of freeze, thaw, and sonication. After centrifugation at 13,000 × *g* for 20 min at 4 °C, the supernatant was incubated with 16 mmol/L 3,3′,5,5′-tetramethylbenzidine and 15 mmol/L H_2O_2, and absorbance at 655 nm was measured for 5 min. MPO activity based on lung tissue protein concentrations was calculated as the changes in absorbance over time. One unit of MPO activity was defined as the change of absorbance of 1.0 per minute. MPO activity was normalized by tissue weight.

2.22. Histopathology examination

The lung tissues were fixed in 4% polyoxymethylene for 1 day and embedded in paraffin blocks before being cut into 5-μm-thick sections. Tissue sections were stained using hematoxylin and eosin. Images were obtained under a light microscope.

2.23. Statistical analysis

All results are presented as mean ± standard error of mean (SEM). One-way ANOVA with Turkey test was used for data analysis. $P < 0.05$ was considered statistically significant. The Prism software (ver. 9.3.1., GraphPad, San Diego, CA) was used for data processing.

3. Results

3.1. fMLFC downregulates cell surface FPR1

Like other GPCRs, FPR1 typically recycles back to the cell surface after agonist-induced receptor internalization[50]. In designing derivatives of the classic formyl tripeptide fMLF for chemical conjugation by adding a C-terminal cysteine, we observed that FPR1 stimulated with this agonist (fMLFC, Fig. 1A) failed to recycle back to the cell surface. To determine FPR1 recycling behavior after treatment with fMLFC, we first confirmed the observed behavior in three types of cells: HeLa FPR1−GFP, transient transfect cells expressing FPR1 with a C-terminally fused GFP; RBL FPR1, a stable cell line expressing FPR1; and HL-60 cells differentiated with DMSO (1.3%, 5 days) to become neutrophil-like (dHL-60) cells[51] Based on flow cytometric analysis of FPR1 that remained on the cell surface 1 h after agonist stimulation, both fMLF and fMLFC induced FPR1 internalization, but more FPR1 was internalized with fMLFC (84%−96%) than fMLF (<60%; Fig. 1B−D), consistent with the higher potency of fMLFC compared with fMLF in chemotaxis (Supporting Information Fig. S1A) and superoxide production (Fig. S1B). The 1 h stimulation time was chosen after conducting time course experiments showing FPR1 internalization appeared 15 min following agonist stimulation and continued to 60 min and beyond. An additional hour was given for the internalized FPR1 to recycle, and a significant difference was observed between fMLF- and fMLFC-treated cells (Fig. 1B−D). Similar results were obtained from confocal microscopy measurement of FPR1 internalization and recycling (Fig. 1E), in which the fMLFC-stimulated cells showed little recycling of the GFP-fused FPR1. In addition to the neutrophil-like dHL-60 cells, the RAW 264.7 mouse macrophage cell line exhibited similar behavior in FPR1 recycling (Supporting Information Fig. S2A). In another experiment, fMLFC was found to be unable to efficiently compete with WKYMVm for binding of FPR2 (Fig. S2B). These results indicate that fMLFC produced stronger internalization of FPR1 but failed its recycling. Several agonist concentrations were tried, and FPR1 internalization was observed with fMLF as low as 100 nmol/L (Fig. S1C). To ensure maximal possible receptor internalization, a higher dose of 5 μmol/L was used throughout the study. In all doses tested, fMLFC exhibited higher potency than fMLF.

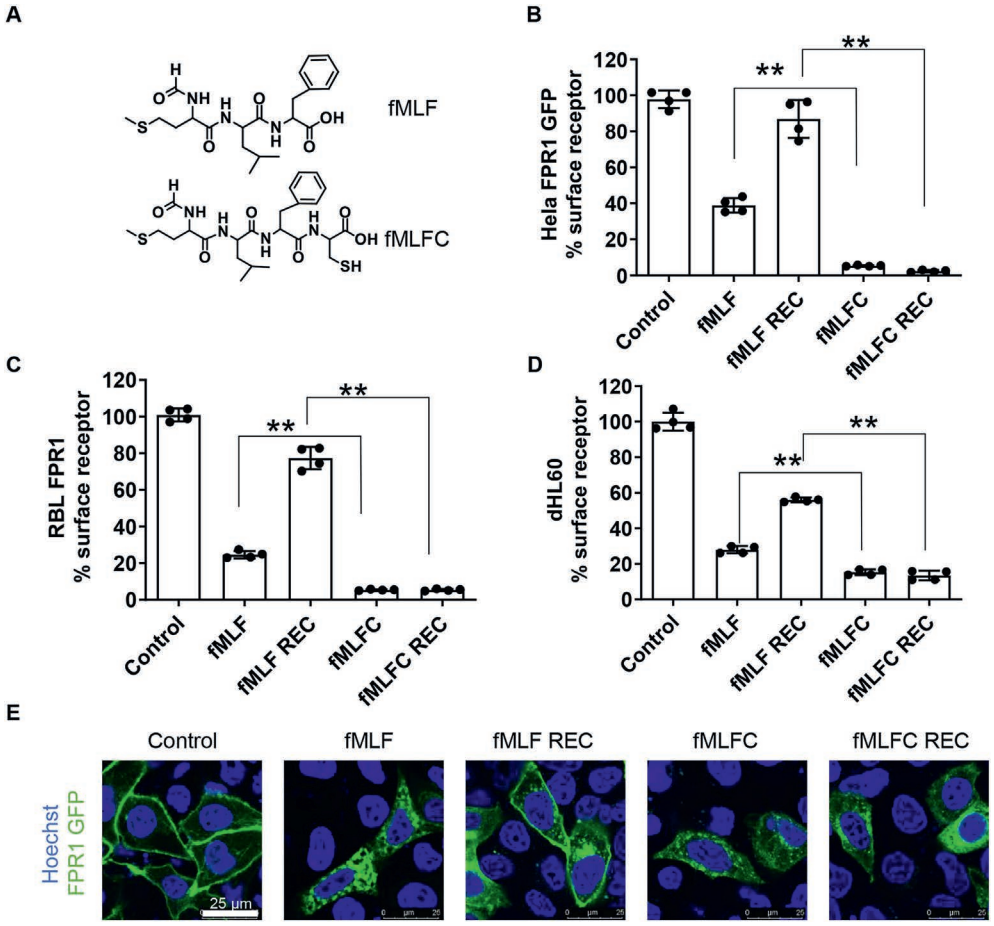

Figure 1 Effect of fMLFC on FPR1 recycling. (A)Structure of fMLF and fMLFC. (B) HeLa FPR1−GFP, (C) RBL FPR1 stable cell line, (D) dHL-60 (differentiated HL-60) cells were treated with 5 μmol/L fMLF or fMLFC for 1 h at 37 °C to induce FPR1 internalization. In the FPR1 recycling group (fMLF REC and fMLFC REC), the cells were washed with PBS and resuspended in complete medium and incubated for 1 h at 37 °C for FPR1 recycling. The cell surface FPR1 was detected with the FPR1 antibody in the APC channel by flow cytometry. Data are presented as mean ± SEM ($n = 4$ independent experiments). $^{**}P < 0.01$. (E) HeLa FPR1−GFP cells were treated with 5 μmol/L fMLF or fMLFC for 1 h at 37 °C to induce FPR1 internalization. In the FPR1 recycling group (fMLF REC and fMLFC REC), the cells were washed with PBS and resuspended in complete medium and incubated for 1 h at 37 °C for FPR1 recycling. Nuclei were stained with 2 μg/mL Hoechst (blue), and FPR1 was tagged with GFP (green). The experiments were performed on the confocal microscope with a 40 × oil objective. Scale bar = 25 μm.

3.2. Effect of RAB proteins on FPR1 recycling

Located in recycling endosomes, the small GTPases RAB4 and RAB11 play an important role in receptor recycling[52]. Wild type (RAB11 WT and RAB4 WT) and dominant negative mutants (RAB11 S25N and RAB4 S22N) were used to study the effect of RAB11 and RAB4 in FPR1 recycling. The dominant negative forms of the RAB proteins were locked in the GDP-bound state and therefore could not be activated[53-55]. Confocal microscopy and flow cytometry were used in the study of RAB for its involvement in FPR1 recycling (Fig. 2A−D). HeLa cells were co-transfected with expression vectors coding for WT RAB4 or WT RAB11 along with the FPR1 expression vector, and the cells were stimulated with fMLF or fMLFC for 1 h to allow receptor endocytosis. As shown in Fig. 2A, WT RAB4 colocalized with FPR1 in fMLF-stimulated cells, and less in fMLFC-stimulated cells. The S22N mutation abrogated RAB4 colocalization with FPR1 (Fig. 2B). For RAB11, the WT form colocalized with FPR1 following stimulation with fMLF but not fMLFC (Fig. 2C), and the colocalization of WT RAB11 with FPR1 was abrogated with the S25N mutation (Fig. 2D). The colocalization data were quantified based on Pearson's correlation coefficient (*R*r) as shown in Fig. 2E, *R*r quantitatively assesses the co-localization of 2 fluorescent proteins[56]. These results demonstrate the involvement of RAB4 and RAB11 in the FPR1 recycling pathway, with RAB11 playing a more critical role. The participation of RAB11 in FPR1 recycling was also confirmed using flow cytometry, which measures cell surface expression of FPR1 after 1 h stimulation with fMLF and 1 h recycling. As shown in Fig. 2F, the S25N mutation of RAB11 negatively affected FPR1 recycling. Taken together, normal FPR1 recycling requires RAB11, and failure to associate with RAB11 might have contributed to the abrogated recycling of FPR1 in fMLFC-stimulated cells. Because of the low-level correlation with fMLFC, subsequent studies have shown in Figs. 2F. Fig. 3B and C showed only the results from fMLF-stimulated cells, in which the difference in RAB mutations and SNX knockdown could be detected.

3.3. Involvement of sorting nexins in FPR1 recycling

To investigate the impact of sorting nexin 3 (SNX3) and sorting nexin 17 (SNX17) on FPR1 recycling, siRNA targeting *SNX17*

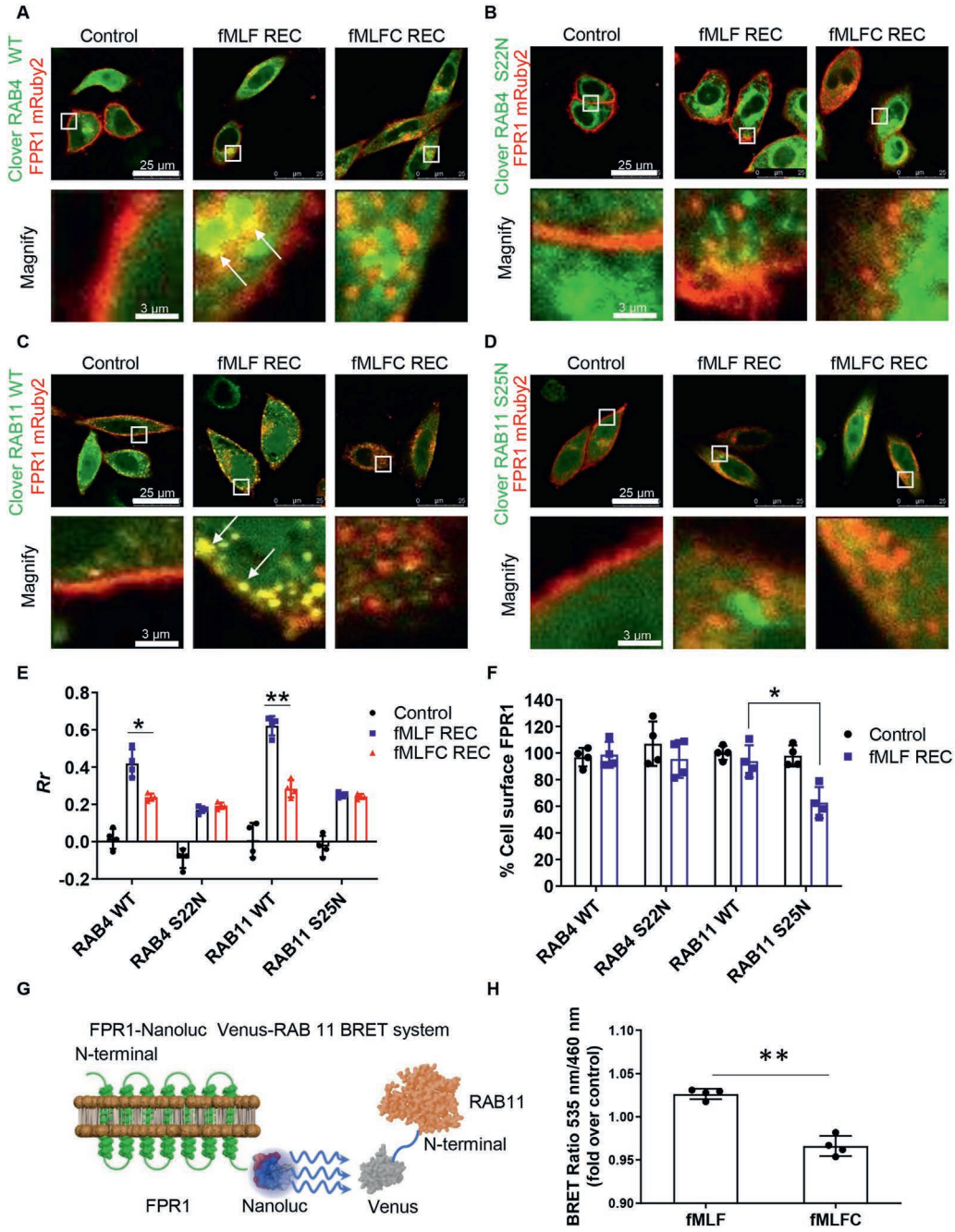

Figure 2 Effect of RAB protein on FPR1 recycling. (A−D) Confocal microscopic images showing colocalization of FPR1 and WT RAB4 (A), S22N RAB4 (B), WT RAB11 (C), and S25N RAB11 (D) 1 h after stimulation with fMLF or fMLFC. FPR1 is shown in red (mRuby2) and RAB in green (Clover), and the overlaid colocalization (yellow) is marked by arrows. Scale bar = 25 and 3 μm. (E) Fluorescence colocalization analysis of (A−D). Pearson's correlation coefficient (*R*r) for colocalization of FPR1 mRuby2 and Clover RAB protein was calculated with the Image J software plugin (Colocalization Finder). (F) Cell surface FPR1 expression based on flow cytometry. HeLa cells expressing mRuby2-labeled FPR1 and Clover-labeled RAB4/RAB11 were treated with 5 μmol/L fMLF for 1 h at 37 °C to induce receptor internalization. In the fMLF REC (recycling) group, the cells were incubated for another 1 h at 37 °C to allow for FPR1 recycling. Cell surface FPR1 was expressed in a bar chart. (G) Schematic diagram of the BRET assay using Nanoluc-tagged FPR1 and Venus-tagged RAB11. (H) HEK293T cells expressing FPR1−Nanoluc and Venus−RAB 11 were stimulated with 5 μmol/L fMLF or fMLFC for 1 h and then treated with the NanoLuc substrate furimazine for 5 min. BRET ratio was recorded at 460 and 515 nm. Data are presented as mean ± SEM (n = 4 independent experiments). *P < 0.05, **P < 0.01.

(si*SNX17*) and *SNX3* (si*SNX3*) were transfected into HeLa cells for knockdown of protein expression (Fig. 3A, showing 86% and 62% decrease in mRNA levels of si*SNX3* and si*SNX17*, respectively). At the end of the recycling period, the FPR1 remaining on the cell surface was significantly lower in the si*SNX17*-treated group than in the control group and the si*SNX3*-

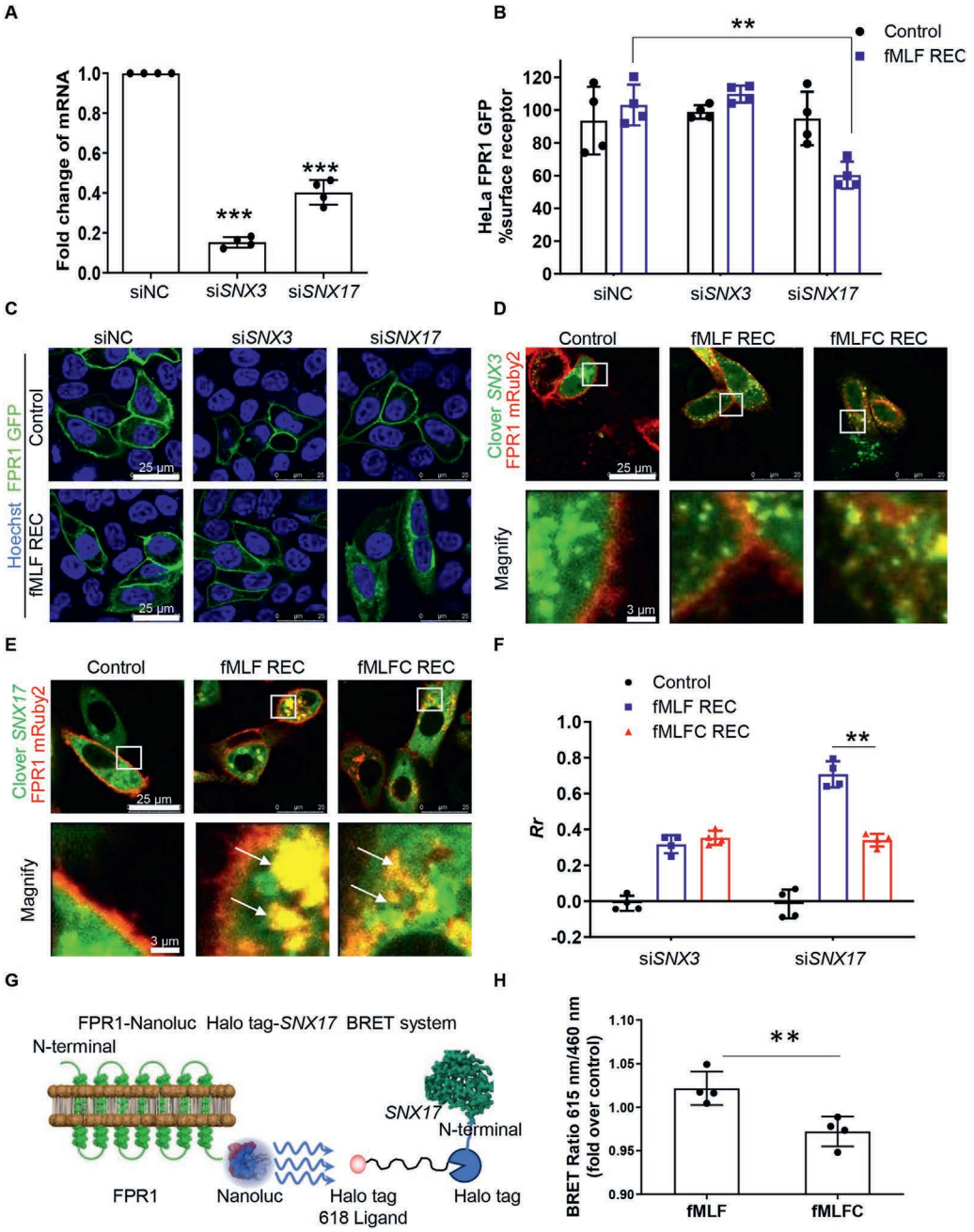

Figure 3 Effect of SNX3 and SNX17 on FPR1 recycling. (A) HeLa cells were transfected with siRNA (siNC as a negative control, si*SNX3* and si*SNX17*) for 48 h at 37 °C to knockdown the SNX expression before transfection with FPR1−GFP. The mRNAs of both si*SNX3* and si*SNX17* were significantly reduced. (B) Cell surface FPR1 expression with control (siNC) and specific siRNA knockdown, after agonist (5 μmol/L fMLF or fMLFC) stimulation for 1 h and recovery for another hour. Cell surface FPR1 expression was significantly reduced in cells receiving si*SNX17* as detected by flow cytometry. (C) Confocal microscopic images showing the effect of siRNA knockdown on FPR1 recycling (1 h), after stimulation with 5 μmol/L fMLF or fMLFC for 1 h at 37 °C to induce FPR1 internalization. Nuclei were stained with Hoechst (blue), and FPR1 was tagged with GFP (green). Scale bar = 25 μm. (D, E) Colocalization of FPR1 and SNX3 (D) or FPR1 and SNX17 (E) in confocal microscopic images. The cells expressing FPR1 mRuby2 and Clover SNX protein were treated with 5 μmol/L fMLF or fMLFC for 1 h at 37 °C to induce FPR1 internalization, and then allowed for FPR1 recycling for 1 h. The green channel was SNX protein (Clover) and the red channel was FPR1 (mRuby2). Colocalization is indicated by yellow (overlay of red and green). Scale bar = 25 μm and 3 μm. (F) Fluorescence colocalization analysis. Pearson's correlation coefficient (*R*r) for colocalization of FPR1 mRuby2 and Clover SNX protein was calculated with Image J software plugin (Colocalization Finder). (G) Schematic diagram of the BRET assay using Nanoluc-tagged FPR1 and HaloTag−SNX17 (Promega). (H) HEK293T cells transfected to express FPR1−Nanoluc and HaloTag−SNX17 were incubated with the HaloTag ligand 618 (the 618 ligand) and then stimulated with either fMLF or fMLFC (5 μmol/L fMLF or fMLFC for 1h). The NanoLuc substrate furimazine was then added, and the BRET ratio was recorded at 460 and 615 nm. Data are presented as mean ± SEM ($n = 4$ independent experiments). $^{**}P < 0.01$.

treated group (Fig. 3B). The results suggested that SNX17 contributed to FPR1 recycling. Additional evidence was obtained from confocal microscopy experiments, showing that FPR1 was mainly localized on plasma membranes in the control group and si*SNX3*-treated group at the end of the recycling period. However, in cells treated with si*SNX17*, FPR1 remained mostly inside the cells (Fig. 3C), suggesting that siRNA knockdown of *SNX17* expression compromised FPR1 recycling to the cell surface. To further investigate the interaction of FPR1 with SNX3 and SNX17, HeLa cells were co-transfected to express FPR1 mRuby2 and Clover SNX3 or Clover SNX17 for confocal microscopy (Fig. 3D and E). There was no clear colocalization between FPR1 and SNX3 in the fMLF- and fMLFC-treated groups (Fig. 3D). The value of *R*r also suggested that the colocalization level between FPR1 and SNX3 was low. There was no significant difference between fMLF and fMLFC in colocalizing with SNX3, as the *R*r values in the fMLF- and fMLFC-treated groups were very close (0.34 and 0.37, respectively; Fig. 3F). There was clear colocalization between FPR1 and SNX17 in the fMLF-treated group (arrows in Fig. 3E), and the *R*r value was 0.72 (Fig. 3F). In comparison, the colocalization level of FPR1 and SNX17 was low in the fMLFC-treated group (Fig. 3E), and the *R*r value was only 0.36 (Fig. 3F). These results are consistent with the findings of flow cytometry (Fig. 3B) and together show that stimulation with fMLF but not fMLFC can engage SNX17 for receptor recycling.

3.4. fMLFC induced lysosomal degradation of FPR1

The above results showed a drastic difference between fMLF and fMLFC in FPR1 recycling, with compromised receptor recycling to the cell surface following fMLFC stimulation. To determine whether the internalized FPR1 was degraded after treatment with fMLFC, the lysosomal inhibitor chloroquine (CQ) was used to investigate the fate of internalized FPR1. The results suggested that fMLFC induced degradation of about 26% of total FPR1 compared with fMLF (16%). CQ inhibited fMLFC-induced FPR1 degradation (Fig. 4A). To validate this result, colocalization of FPR1 with different degradation pathway markers was determined using confocal microscopy. In the lysosome degradation pathway, the target protein first enters the early endosome, then the late endosome, and the lysosome. RAB5, RAB7, and LAMP1 are markers of the early endosome, late endosome, and lysosome, respectively[57-59]. All these proteins were fused with fluorescence proteins for confocal microscopy. There was a high level of colocalization between RAB5 and FPR1 after treatment with fMLF and fMLFC (Fig. 4B). The *R*r value (0.74 in the fMLF-treated group and 0.70 in the fMLFC-treated group) also supported the colocalization of RAB5 with FPR1 (Fig. 4E). However, colocalization of FPR1 with RAB7 and LAMP1 in the fMLFC-treated group was much higher than in the fMLF-treated group (Fig. 4C and D). The *R*r value in the fMLFC-treated group was also higher than that in the fMLF-treated group (Fig. 4E). Inhibition of proteasome (by MG132) and disruption of autophagy (bafilomycin) did not significantly rescue FPR1 degradation (Fig. S2C). These results demonstrated that in fMLF-stimulated cells, FPR1 entered the early endosome, where it interacted with RAB11 and SNX17 before recycling back to the cell surface. In fMLFC-treated cells, FPR1 also entered the early endosome, but most of the receptors subsequently entered the late endosome and lysosome for degradation instead of recycling back to the cell surface.

3.5. Cryo-EM structure of the fMLFC−FPR1−Gi−scFv16 complex

To determine the structural difference between fMLF and fMLFC in FPR1 binding, the fMLFC−FPR1−Gi complex was prepared (Supporting Information Figs. S3 and S4) and its structure was determined by cryo-EM to an overall resolution of 3.03 Å (Fig. 5A and B, Table S1). The antibody fragment scFv16 was used for stabilization of the fMLFC−FPR1−Gi complex. The ligand-binding pocket of FPR1 was surrounded by transmembrane (TM) helices 2, 3, 5, and 6, with minor involvement of TM7 (Fig. 5A and B). fMLFC assumes a pose with its N-terminus inserted into the binding pocket, similar to that of fMLF (PDB accession number 7EUO[48]). The fMLF-interacting residues in the FPR1 structural model include F81, V105, D106, L109, F110, V113, R201, R205, W254, Y257, Q258, and T265 (Fig. 5C). In the fMLFC−FPR1−Gi structural model, in addition to the above-mentioned residues on FPR1, the cysteine in the C-terminus of fMLFC interacts with F102, T177 and F178 (Fig. 5D). Following FPR1 structural analysis, alanine substitution of these residues (F102A, T177A and F178A) was conducted to confirm their functional interaction with fMLFC. Results from receptor recycling assay showed that alanine substitution of these residues (F102A, T177A and F178A) increased recycling of the FPR1 mutants to the cell surface (Fig. 5E). These results indicate that the additional contacts of FPR1 for fMLFC may contribute to its higher potency than fMLF and the resulting phenotype of FPR1 recycling.

3.6. fMLFC induced characteristic changes in FPR1 conformation

Different conformational changes of a receptor underline different cellular activities[60]. Therefore, it was further postulated that fMLFC could induce conformational changes of FPR1 that differ from those induced by fMLF. To test this hypothesis, fluorescent biosensors were prepared by fusion of a NanoLuc protein to the C terminus of FPR1 with simultaneous insertion of a FlAsH-binding motif (Cys−Cys−Pro−Gly−Cys−Cys) into the three individual ICLs (Fig. 5F, schematic of FPR1-FlAsH-ICL3-NanoLuc biosensor). The agonist-induced conformational changes could be measured based on changes in the distance between the FlAsH-binding motif and the Nanoluc, as reflected in changes in the intensity of BRET. Stimulation with fMLFC resulted in robust BRET between the inserted FlAsH binding motif and the NanoLuc (Fig. 5G and H), suggesting a conformational change with an increased distance between the three ICLs and the C-terminus of FPR1. Although the intensity change was the smallest with the ICL1 biosensor, the BRET ratio of fMLFC/fMLF was the highest, indicating maximal change in receptor conformation induced by fMLFC treatment. Of interest, fMLF induced little BRET in the FPR1-FlAsH-ICL1-NanoLuc biosensor (Fig. 5G and H). These results demonstrated that fMLFC can induce different conformational changes of FPR1 compared with fMLF, thus leading to different downstream signaling.

3.7. Correlation of FPR1 conformational change with its recycling

The correlation of FPR1 recycling with receptor conformational changes induced by fMLF and fMLFC was investigated. Using the BRET proximity assay, we determined the affinity of FPR1, in one

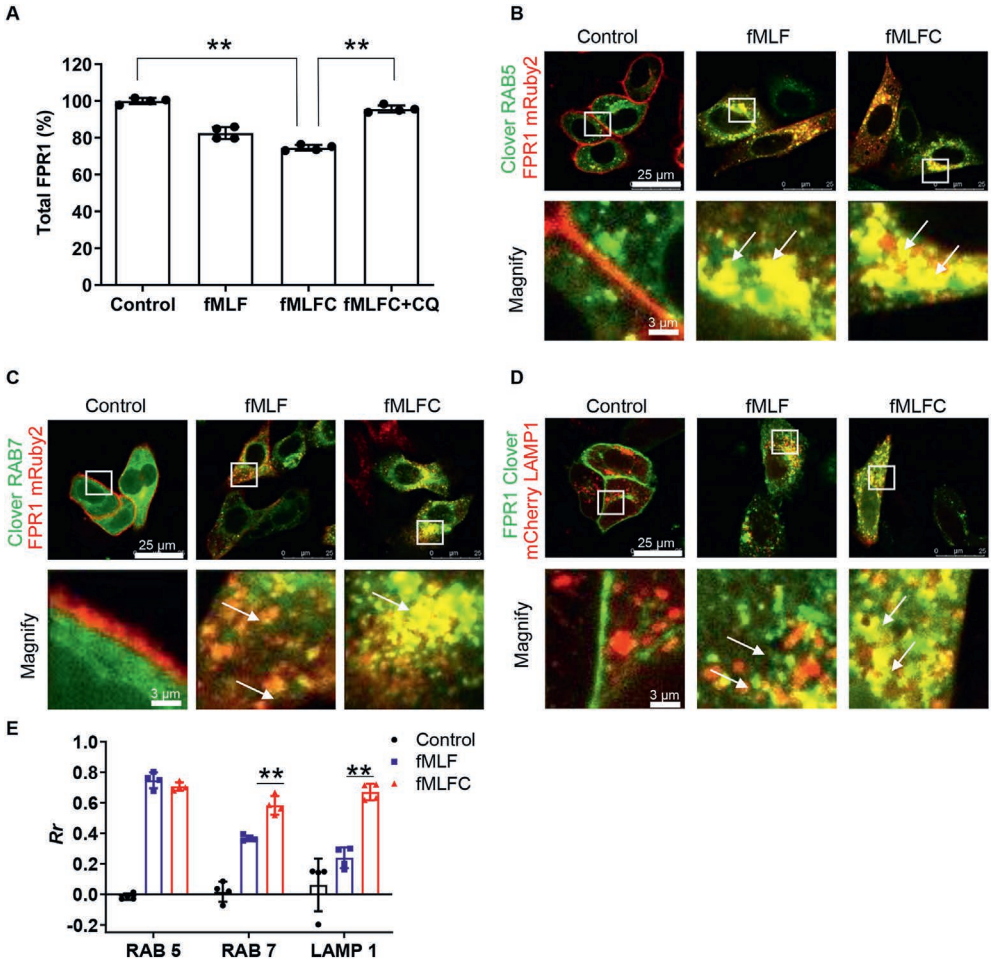

Figure 4 FPR1 degradation pathways. (A) fMLFC induced FPR1 degradation. HeLa cells expressing FPR1−GFP were pre-incubated with 1 μmol/L cycloheximide for 1 h, and then were added 5 μmol/L fMLF or fMLFC with or without 30 μmol/L lysosomal inhibitor chloroquine (CQ) for another 9 h of incubation at 37 °C. Then, the remaining FPR1−GFP was detected based on green fluorescence by flow cytometry. (B−D), colocalization of FPR1 with the early endosome marker RAB5 (B), the late endosome marker RAB7. (C) And the lysosome marker LAMP1 (D), These markers were fluorescent-tagged fusion proteins as marked and co-transfected with FPR1 for 24 h at 37 °C. The experiments were performed on a confocal microscope. Scale bar = 25 and 3 μm. (E) Fluorescence colocalization analysis. Pearson's correlation coefficient (*R*r) for colocalization of FPR1 and RAB5, RAB7 or LAMP1 were calculated with Image J software plugin (Colocalization Finder). Data are presented as mean ± SEM ($n = 4$ independent experiments). $^{**}P < 0.01$.

of the conformations induced by fMLF or fMLFC, for SNX17 and RAB11. The human FPR1 was attached in its C-terminus with a NanoLuc, the SNX17 was tagged with the HaloTag and RAB11 was fused to the Venus fluorescent protein (Figs. 3G and 2G). After stimulation with 5 μmol/L fMLF or fMLFC, BRET was measured, and the ratios (615/460 nm for HaloTag, 515/460 nm for Venus) were compared (Figs. 3H and 2H). With both constructs, fMLF recruited more SNX17 and RAB11 than fMLFC, indicating more efficient recycling of the receptor.

3.8. fMLFC ameliorated inflammatory lung injury in LPS-treated mice

In acute lung injury, neutrophil infiltration into lung tissue results in lung vascular injury[61]. FPR1 is expressed at high levels on the neutrophil cell surface and contributes to neutrophil recruitment to the site of inflammation[62]. At higher concentrations of chemoattractants, including formyl peptides, FPR1 mediates superoxide generation and granule enzyme release, which contribute directly to acute lung injury[63]. As mentioned above, fMLFC treatment decreases cell surface expression of FPR1. Therefore, it is of interest to determine whether fMLFC could influence inflammatory tissue injury in mice. An LPS-induced acute lung injury model was used to test this hypothesis. In mice receiving tail vein injection of fMLFC, neutrophil cell surface expression of mouse FPR1 was significantly reduced (Fig. 6A). Intratracheal administration of LPS led to acute lung injury, and neutrophils were the first type of cells recruited to the injury site[63]. Neutrophil infiltration could be measured by tissue MPO contents, which come mostly from neutrophils but can come from macrophages to a lesser extent in acute lung injury. The LPS-induced elevation of MPO activity was seen in the mouse model (Fig. 6B), but diminished in the lung tissue from mice pretreated with fMLFC (Fig. 6B). The histology of the mouse lung sections after LPS treatment for 6 h revealed neutrophil infiltration (Fig. 6C). Again, fMLFC pretreatment reduced neutrophil infiltration and restored lung tissue architecture compared with the LPS-only group. Of interest, tail vein injection of fMLFC alone increased neutrophils

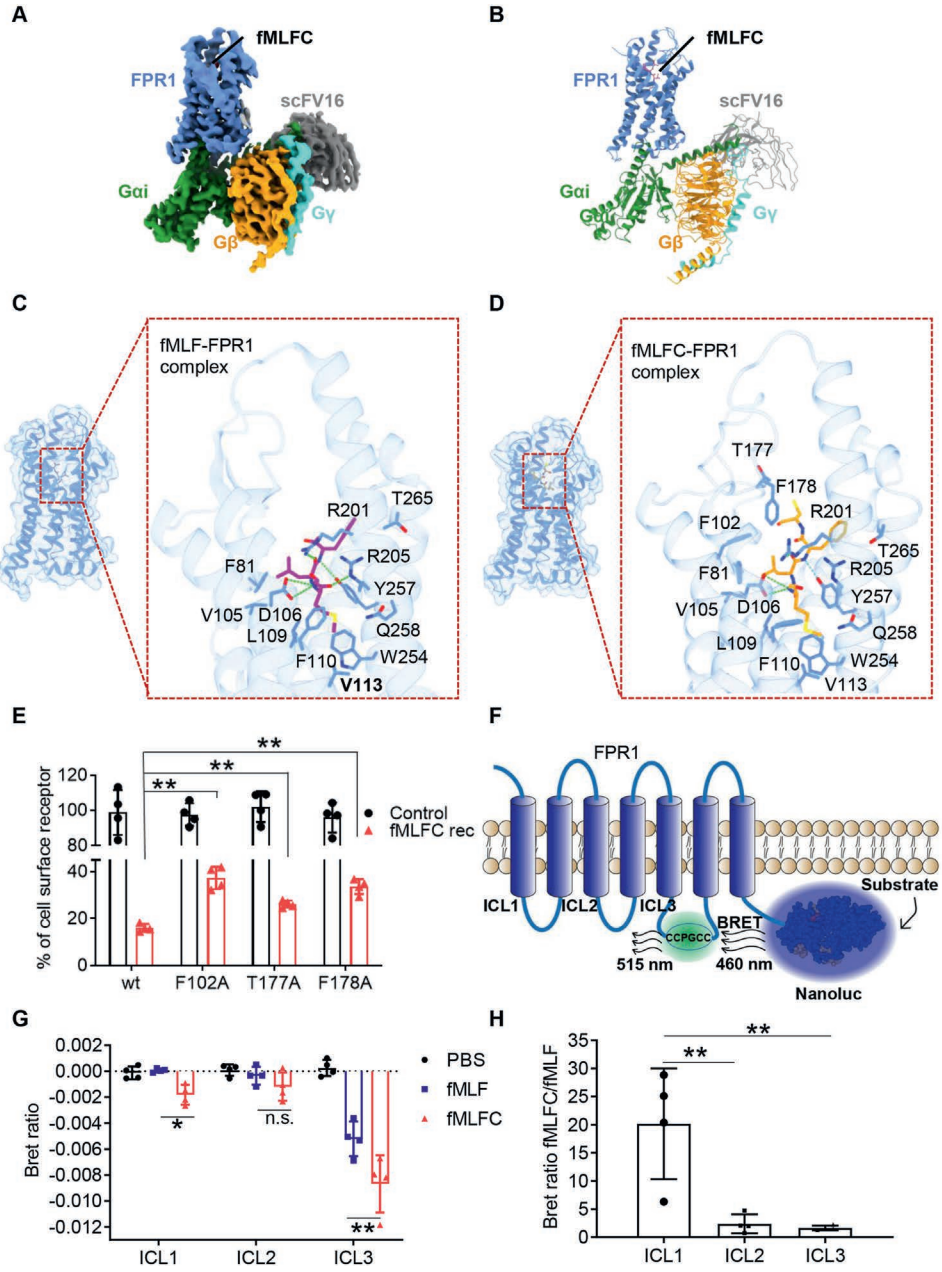

Figure 5 Cryo-EM structure and conformational changes of fMLFC-bound FPR1. Cryo-EM density map (A) and structural model (B) of the fMLFC−FPR1−Gi−scFv16 complex in side view. Overall structure of fMLF−FPR1−Gi−scFv16 complex (C) and fMLFC−FPR1−Gi−scFv16 complex (D) from side view (Left) and key interaction residues (Inset at Right). (E) Effects of key residue mutation on FPR1 recycling. HeLa cells were transfected with FPR1 mutants (F102A, T177A, F178A) predicted to interact with fMLFC. The cells were treated with 5 μmol/L fMLFC for 1 h, and mutant FPR1 recycling was measured for another h. Cell surface FPR1 was detected using flow cytometry. (F) Schematic of FlAsH NanoBRET-based FPR1 biosensor (FPR1-FlAsH-ICL3-NanoLuc). (G) Conformational changes of FlAsH NanoBRET-based FPR1 biosensors in response to fMLF and fMLFC. HeLa cells were transfected with FPR1-FlAsH-ICL1-NanoLuc, FPR1-FlAsH-ICL2-NanoLuc, FPR1-FlAsH-ICL1-NanoLuc incubate for 24 h. Then cells were treated with 1 μmol/L FlAsH dye for 1 h and then incubated with 5 μmol/L Coelenterazine H for 5 min fMLF (5 μmol/L), fMLFC (5 μmol/L), or PBS were added to the cell solution, and the BRET ratio was recorded. (H) BRET ratio of fMLFC/BRET ratio of fMLF from the (G). Data are presented as mean ± SEM ($n = 4$ independent experiments). *$P < 0.05$, **$P < 0.01$; n.s., no significance.

in the lung tissue section (Fig. 6C) since fMLFC is a strong chemoattractant and its presence in pulmonary tissue following tail vein injection may attract neutrophils at the beginning. However, overall MPO level in the lung tissue was not significantly changed in the fMLFC-only group (Fig. 6B), and fMLFC-induced FPR1 internalization eventually reduced available FPR1 on the cell surface, thereby reducing neutrophil proinflammatory responses. This effect was demonstrated *in vitro* in dHL-60 cells. The cells preincubated with fMLFC for 1 h lost responsiveness to subsequent fMLF stimulation in the superoxide production assay

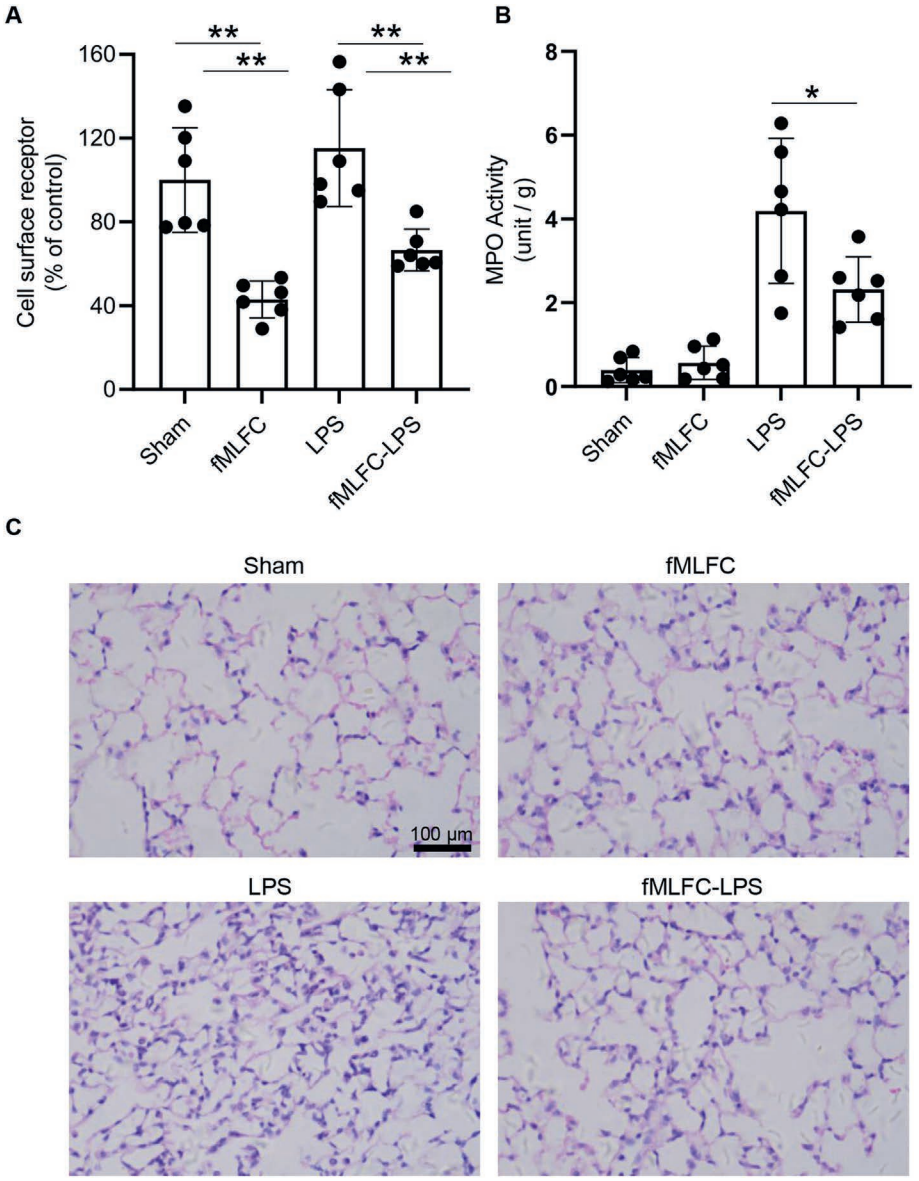

Figure 6 fMLFC ameliorates lung injury in LPS-treated mice. The mice were divided into four groups: sham, fMLFC only (4 mg/kg, tail vein injection), LPS only (2 mg/kg, intratracheal inoculation, 6 h), and fMLFC−LPS (4 mg/kg fMLFC tail vein injection for 1 h, then 2 mg/kg LPS intratracheal inoculation for 6 h). (A) Mouse neutrophil surface FPR1 detection. The FPR1 on the neutrophil cell membrane was labeled with 250 nmol/L fMLFIIK−FITC for 1 h on ice. Then the FPR1 on the cell surface were quantified by flow cytometry. (B) MPO activity. (C) Photomicrograph of hematoxylin-eosin-stained lung sections by light microscopy, Scale bar, 100 μm. Data are presented as mean ± SEM from 6 mice in each group. $*P < 0.05$, $**P < 0.01$.

(Fig. S2D). These results indicate that fMLFC can ameliorate acute lung injury by reducing cell surface expression of FPR1 in phagocytes.

4. Discussion

In the present study, we have identified a formyl peptide, fMLFC, that effectively reduces cell surface FPR1 expression by preventing its recycling after endocytosis. Additionally, fMLFC has been found to inhibit dHL-60 cell migration and reduce neutrophil infiltration in a mouse model of acute lung injury.

The formylated tripeptide fMLF was identified as an *E. coli*-derived agonist for FPR1[64]. In our study, a cysteine was added to the C-terminus of fMLF for drug conjugation. The resulting fMLFC is about one order of magnitude more potent than fMLF in the Ca^{2+} mobilization assay and displays higher affinity for FPR1 in the competitive binding assay[45]. However, in a competitive binding assay, fMLFC did not effectively compete with WKYMVm for FPR2 binding. No dimerization was found between FPR1 and FPR2 upon stimulation with fMLF or fMLFC (Fig. S2E). The present study was based on our observation that FPR1 failed to recycle back to the cell surface after fMLFC treatment. The phenomenon of distinct intracellular fates caused

by different ligands has been reported for other receptors. For instance, the glucose-dependent insulinotropic polypeptide receptor (GIPR) was constitutively internalized and recycled to the cell surface. GIPR was observed to undergo a change from a fast recycling pathway to a slow *trans*-Golgi network pathway after being stimulated with glucose-dependent insulinotropic polypeptide[65]. Similarly, ultraviolet light C and cisplatin were found to alter the intracellular traffic routes of the EGF receptor. Instead of degrading or recycling back to the plasma membrane, the EGF receptor accumulated in a lysobisphosphatidic acid-rich compartment after ultraviolet light C and cisplatin treatment[66]. Aminooxypentane-RANTES (AOP-RANTES, a modified CC chemokine RANTES) rapidly caused a 90% decrease in cell surface expression of CCR5 in lymphocytes, monocytes, and macrophages due to inhibition of recycling of the internalized CCR5, whereas RANTES did not[67].

In the present study, RAB4, RAB11, SNX3, and SNX17 were investigated for their roles in FPR1 recycling[14,17,47]. Several approaches were taken, including null mutations of the small GTPase and siRNA-mediated knockdown of the SNXs. The combined use of confocal microscopy and flow cytometry led to the identification of RAB11 and SNX17 as participating factors for FPR1 recycling in the fMLF-treated group. Colocalization of FPR1 with RAB11 was abrogated when a null mutation (S25N) was introduced into RAB11, consistent with its role in FPR1 recycling to the cell surface. siRNA-dependent knockdown of SNX17, but not SNX3, affected FPR1 recycling in fMLF-stimulated cells. In contrast, fMLFC stimulation negatively affected FPR1 colocalization with SNX17. These findings provide mechanistic insights into the reduction in FPR1 recycling after fMLFC stimulation.

Degradation of GPCRs such as FPR1 contributes to loss of receptor on the cell surface of neutrophils and other types of cells, including endothelial and epithelial cells[68]. In this study, the results showed that FPR1 enters 2 different intracellular traffic routes after being treated with fMLF and fMLFC. FPR1 could enter the early endosome in both fMLF- and fMLFC-treated cells, as evidenced by receptor colocalization with the early endosome marker RAB5. The intracellular traffic routes then diverge with the fMLF-treated receptor entering the recycling pool, where it interacts with RAB11 and SNX17. Conversely, in the fMLFC-treated group. FPR1 enters the late endosome (colocalized with late endosome marker RAB7) and lysosome (colocalized with the lysosome marker LAMP1) for degradation. The significant loss of cell surface FPR1 in the fMLFC-treated group suggests that most of the internalized FPR1 is retained intracellularly, with only a small fraction entering the lysosome degradation pathway. In our study, the use of MG132 and bafilomycin did not effectively prevent FPR1 degradation.

Previous studies have shown that GPCRs can enter into an unresponsive state following agonist stimulation, a phenomenon termed desensitization[69]. GPCR desensitization is associated with GRK-dependent phosphorylation and β-arrestin binding[70], which are generally applicable to GPCRs, including FPR1[71]. Desensitization may be attributable, at least in part, to the loss of cell surface receptors due to agonist-induced internalization[72]. The structural determinants for downstream pathways remain unclear at present. We therefore sought to determine the structure of fMLFC-bound FPR1 in the active state (Gi protein-coupled). Our structural model showed common features shared between the fMLF- and fMLFC-bound FPR1, including strong interaction of the formyl-Met with the D106/R201/R205 triad[48]. However, the C-terminal cysteine forms additional contacts with F102/T177/F178, and the correlation of these interactions with receptor recycling was confirmed in cells expressing the alanine-substituted mutants. This finding provides a clue to the structural basis for the different trafficking pattern of the internalized FPR1 when it binds fMLFC. Extending this result, we constructed FlAsH nanoBRET biosensors to detect conformational changes induced by fMLF and fMLFC. Our results showed that the fMLFC-induced FPR1 conformational change differs from that induced by fMLF, supporting the notion that agonist-induced FPR1 conformational change underlines the fate of the internalized receptor. Indeed, our BRET proximity assay has shown that the fMLF-stimulated receptor associates favorably with the recycling-related proteins SNX17 and RAB11, while the fMLFC-stimulated receptor lags. These findings provide an underlying mechanism by which fMLF induces FPR1 conformational changes and a strong association with the SNX17 and the small GTPase RAB11.

In summary, the present study employs multiple experimental approaches to characterize the fMLF- and fMLFC-stimulated FPR1 internalization, its recycling, and lysosomal degradation. The study has potential application value to the control of inflammation, in which neutrophil infiltration and activation play a role. This study is limited by presently unidentified factors that link receptor conformational change to the choice of different recycling routes for the internalized FPR1. Moreover, administration of fMLFC after establishment of the acute lung injury model would have more practical value in clinical treatment and should be explored in the future. Further studies will be required to delineate the pathways and mechanisms that determine the fate of the internalized receptor, which may better guide the development of therapeutic approaches based on targeted removal of cell surface receptors.

5. Conclusions

The present study has identified fMLFC as a potential chemical knockdown reagent for reducing cell surface FPR1. Our findings indicate that fMLFC decreases the interaction of FPR1 with recycling-related proteins (RAB11 and SNX17) while increasing its interaction with degradation-related proteins (RAB7 and LAMP1). As a result, fMLFC reduces cell surface FPR1 and induces the degradation of a portion of FPR1 through lysosomes. Furthermore, a solved cryo-EM structure of fMLFC−FPR1 complex has revealed that the cystine on the C-terminus of fMLFC interacts with additional amino acids (F102A, T177A, and F178A) in the binding pocket of FPR1, thus contributing to conformational changes that may lead to interaction of FPR1 with degradation-related proteins and impede its interaction with recycling-related proteins. We have shown that fMLFC can alleviate LPS-induced acute lung injury in a mouse model, suggesting potential therapeutic application of fMLFC in treating inflammatory diseases, in which neutrophil infiltration plays a role.

Ethical statement

The mouse studies were approved by the Institutional Animal Care and Use Committee of The Chinese University of Hong Kong, Shenzhen, China (Protocol Number: AE2021013).

Data and code availability

The Cryo-EM structure of fMLF−FPR1−Gi complex has been deposited in the PDB with the accession code PDB: 7EUO. The PDB code of fMLFC−FPR1−Gi complex Cryo-EM structure is: 9KFT.

Acknowledgments

We thank the Kobilka Cryo-Electron Microscopy Center in the Chinese University of Hong Kong, Shenzhen, for cryo-electron microscopy analysis, and Prof. Guangpu Li of the University of Oklahoma College of Medicine for plasmids of Rab GTPases. This work was supported in part by grants from the National Natural Science Foundation of China 82302448 (Junlin Wang) and 32070950 (Richard D. Ye), the Shenzhen Fundamental Research Program SGDX20210823103804030 (Jiahong Lu and Richard D. Ye, China), the Science and Technology Development Fund, Macau SAR 0025/2022/A1 and 0128/2019/A3 (Jiahong Lu, China), Yunnan Key Research and Development Program Grant (No. 202402AA310032, Richard D. Ye, China), and fund from Shenzhen-Hong Kong Cooperation Zone for Technology and Innovation (No. HZQB-KCZYB-2020056, China). The work was also supported by the Fellowship of China Postdoctoral Science Foundation 2021M703092 (Junlin Wang).

Author contributions

Richard D. Ye and Junlin Wang designed research; Junlin Wang, Qiwen Liao, Geng Chen, Yixin Chang performed research; Jiahong Lu, Hong Nie and Richard D. Ye supervised research; Richard Ye and Junlin Wang wrote the paper.

Conflicts of interest

The authors declare no conflicts of interest.

Appendix A. Supporting information

Supporting information to this article can be found online at https://doi.org/10.1016/j.apsb.2026.03.019.

References

1. Gurevich VV, Gurevich EV. GPCR signaling regulation: the role of GRKs and arrestins. *Front Pharmacol* 2019;**10**:125.
2. Pavlos NJ, Friedman PA. GPCR signaling and trafficking: the long and short of it. *Trends Endocrinol Metab* 2017;**28**:213−26.
3. Zhu CH, Lan XB, Wei ZQ, Yu JQ, Zhang J. Allosteric modulation of G protein-coupled receptors as a novel therapeutic strategy in neuropathic pain. *Acta Pharm Sin B* 2024;**14**:67−86.
4. Yang H, Wang Y, Liu W, He T, Liao J, Qian Z, et al. Genome-wide pan-GPCR cell libraries accelerate drug discovery. *Acta Pharm Sin B* 2024;**14**:4296−311.
5. Vines CM, Revankar CM, Maestas DC, LaRusch LL, Cimino DF, Kohout TA, et al. N-formyl peptide receptors internalize but do not recycle in the absence of arrestins. *J Biol Chem* 2003;**278**:41581−4.
6. Harding C, Heuser J, Stahl P. Receptor-mediated endocytosis of transferrin and recycling of the transferrin receptor in rat reticulocytes. *J Cell Biol* 1983;**97**:329−39.
7. Davis CG, Goldstein JL, Sudhof TC, Anderson RG, Russell DW, Brown MS. Acid-dependent ligand dissociation and recycling of LDL receptor mediated by growth factor homology region. *Nature* 1987;**326**:760−5.
8. Seachrist JL, Ferguson SS. Regulation of G protein-coupled receptor endocytosis and trafficking by Rab GTPases. *Life Sci* 2003;**74**:225−35.
9. Grant BD, Donaldson JG. Pathways and mechanisms of endocytic recycling. *Nat Rev Mol Cell Biol* 2009;**10**:597−608.
10. Ward ES, Martinez C, Vaccaro C, Zhou J, Tang Q, Ober RJ. From sorting endosomes to exocytosis: association of Rab4 and Rab11 GTPases with the Fc receptor, FcRn, during recycling. *Mol Biol Cell* 2005;**16**:2028−38.
11. McCaffrey MW, Bielli A, Cantalupo G, Mora S, Roberti V, Santillo M, et al. Rab4 affects both recycling and degradative endosomal trafficking. *FEBS Lett* 2001;**495**:21−30.
12. Odley A, Hahn HS, Lynch RA, Marreez Y, Osinska H, Robbins J, et al. Regulation of cardiac contractility by Rab4-modulated beta2-adrenergic receptor recycling. *Proc Natl Acad Sci U S A* 2004;**101**:7082−7.
13. Parent A, Hamelin E, Germain P, Parent JL. Rab11 regulates the recycling of the β2-adrenergic receptor through a direct interaction. *Biochem J* 2009;**418**:163−72.
14. Li H, Li HF, Felder RA, Periasamy A, Jose PA. Rab4 and Rab11 coordinately regulate the recycling of angiotensin II type I receptor as demonstrated by fluorescence resonance energy transfer microscopy. *J Biomed Opt* 2008;**13**:031206.
15. Weeratunga S, Paul B, Collins BM. Recognising the signals for endosomal trafficking. *Curr Opin Cell Biol* 2020;**65**:17−27.
16. Tian Y, Kang Q, Shi X, Wang Y, Zhang N, Ye H, et al. SNX-3 mediates retromer-independent tubular endosomal recycling by opposing EEA-1-facilitated trafficking. *PLoS Genet* 2021;**17**:e1009607.
17. Chen C, Garcia-Santos D, Ishikawa Y, Seguin A, Li L, Fegan KH, et al. Snx3 regulates recycling of the transferrin receptor and iron assimilation. *Cell Metab* 2013;**17**:343−52.
18. Rivero-Rios P, Tsukahara T, Uygun T, Chen AL, Chavis GD, Giridharan SSP, et al. Recruitment of the SNX17−Retriever recycling pathway regulates synaptic function and plasticity. *J Cell Biol* 2023;**222**:29.
19. Boldicke T. Blocking translocation of cell surface molecules from the ER to the cell surface by intracellular antibodies targeted to the ER. *J Cell Mol Med* 2007;**11**:54−70.
20. Martin NP, Lefkowitz RJ, Shenoy SK. Regulation of V2 vasopressin receptor degradation by agonist-promoted ubiquitination. *J Biol Chem* 2003;**278**:45954−9.
21. Walrafen P, Verdier F, Kadri Z, Chretien S, Lacombe C, Mayeux P. Both proteasomes and lysosomes degrade the activated erythropoietin receptor. *Blood* 2005;**105**:600−8.
22. Shenoy SK, Xiao K, Venkataramanan V, Snyder PM, Freedman NJ, Weissman AM. Nedd4 mediates agonist-dependent ubiquitination, lysosomal targeting, and degradation of the β2-adrenergic receptor. *J Biol Chem* 2008;**283**:22166−76.
23. Zhang L, Wang H, Yang T, Su Z, Fang D, Wang Y, et al. Formylpeptide receptor 1 mediates the tumorigenicity of human hepatocellular carcinoma cells. *OncoImmunology* 2016;**5**:e1078055.
24. Alu A, Han X, Ma X, Wu M, Wei Y, Wei X. The role of lysosome in regulated necrosis. *Acta Pharm Sin B* 2020;**10**:1880−903.
25. Luzio JP, Pryor PR, Bright NA. Lysosomes: fusion and function. *Nat Rev Mol Cell Biol* 2007;**8**:622−32.
26. Huber LA, Teis D. Lysosomal signaling in control of degradation pathways. *Curr Opin Cell Biol* 2016;**39**:8−14.
27. Pushparaj PN, Aarthi JJ, Manikandan J, Kumar SD. siRNA, miRNA, and shRNA: *in vivo* applications. *J Dent Res* 2008;**87**:992−1003.
28. Miao Y, Fu C, Yu Z, Yu L, Tang Y, Wei M. Current status and trends in small nucleic acid drug development: leading the future. *Acta Pharm Sin B* 2024;**14**:3802−17.
29. Iwamoto N, Sumi D, Ishii T, Uchida K, Cho AK, Froines JR, et al. Chemical knockdown of protein-tyrosine phosphatase 1B by 1,2-naphthoquinone through covalent modification causes persistent transactivation of epidermal growth factor receptor. *J Biol Chem* 2007;**282**:33396−404.

30. Sun X, Wang J, Yao X, Zheng W, Mao Y, Lan T, et al. A chemical approach for global protein knockdown from mice to non-human primates. *Cell Discov* 2019;**5**:10.
31. Peng L, Zhang Z, Lei C, Li S, Zhang Z, Ren X, et al. Identification of new small-molecule inducers of estrogen-related receptor alpha (ERRalpha) degradation. *ACS Med Chem Lett* 2019;**10**:767−72.
32. Li C, Lin Y, Chen Y, Song X, Zheng X, Li J, et al. A specific mini-intrabody mediates lysosome degradation of mutant Huntingtin. *Adv Sci (Weinh)* 2023;**10**:e2301120.
33. Marschall AL, Dubel S, Boldicke T. Specific *in vivo* knockdown of protein function by intrabodies. *mAbs* 2015;**7**:1010−35.
34. Békés M, Langley DR, Crews CM. PROTAC targeted protein degraders: the past is prologue. *Nat Rev Drug Discov* 2022;**21**: 181−200.
35. Peng X, Hu Z, Zeng L, Zhang M, Xu C, Lu B, et al. Overview of epigenetic degraders based on PROTAC, molecular glue, and hydrophobic tagging technologies. *Acta Pharm Sin B* 2024;**14**:533−78.
36. Lewis MJ, Pelham H. Ligand-induced redistribution of a human KDEL receptor from the Golgi complex to the endoplasmic reticulum. *Cell* 1992;**68**:353−64.
37. Yuan ZC, Zeng N, Liu L, Wang T, Dai LQ, Wang H, et al. Mitochondrial damage-associated molecular patterns exacerbate lung fluid imbalance *via* the formyl peptide receptor-1 signaling pathway in acute lung injury. *Crit Care Med* 2021;**49**:e53−62.
38. Liu M, Zhao J, Chen K, Bian X, Wang C, Shi Y, et al. G protein-coupled receptor FPR1 as a pharmacologic target in inflammation and human glioblastoma. *Int Immunopharmacol* 2012;**14**:283−8.
39. Ge Y, Guan H, Li T, Wang J, Ying L, Guo S, et al. Discovery of Yersinia LcrV as a novel biased agonist of formyl peptide receptor 1 to bi-directionally modulate intracellular kinases in triple-negative breast cancer. *Acta Pharm Sin B* 2025;**15**:3646−62.
40. Yang X, Xiao W, Le Q, Zhang Z, Wang W, Lee SH, et al. Knockout of formyl peptide receptor 1 reduces osteogenesis and bone healing. *Life Sci* 2024;**344**:122583.
41. Schepetkin IA, Kirpotina LN, Khlebnikov AI, Cheng N, Ye RD, Quinn MT. Antagonism of human formyl peptide receptor 1 (FPR1) by chromones and related isoflavones. *Biochem Pharmacol* 2014;**92**: 627−41.
42. Ahmet DS, Basheer HA, Salem A, Lu D, Aghamohammadi A, Weyerhäuser P, et al. Application of small molecule FPR1 antagonists in the treatment of cancers. *Sci Rep* 2020;**10**:17249.
43. He HQ, Ye RD. The formyl peptide receptors: diversity of ligands and mechanism for recognition. *Molecules* 2017;**22**:455.
44. Niedel JE, Kahane I, Cuatrecasas P. Receptor-mediated internalization of fluorescent chemotactic peptide by human neutrophils. *Science* 1979;**205**:1412−4.
45. Wang J, Chen M, Li S, Ye RD. Targeted delivery of a ligand−drug conjugate via formyl peptide receptor 1 through cholesterol-dependent endocytosis. *Mol Pharm* 2019;**16**:2636−47.
46. Pons V, Luyet PP, Morel E, Abrami L, van der Goot FG, Parton RG, et al. Hrs and SNX3 functions in sorting and membrane invagination within multivesicular bodies. *PLoS Biol* 2008;**6**:e214.
47. van Kerkhof P, Lee J, McCormick L, Tetrault E, Lu W, Schoenfish M, et al. Sorting nexin 17 facilitates LRP recycling in the early endosome. *EMBO J* 2005;**24**:2851−61.
48. Chen G, Wang X, Liao Q, Ge Y, Jiao H, Chen Q, et al. Structural basis for recognition of N-formyl peptides as pathogen-associated molecular patterns. *Nat Commun* 2022;**13**:5232.
49. Wang J, Chen G, Liao Q, Lyu W, Liu A, Zhu L, et al. Cryo-EM structure of the human chemerin receptor 1-Gi protein complex bound to the C-terminal nonapeptide of chemerin. *Proc Natl Acad Sci U S A* 2023;**120**:e2214324120.
50. Key TA, Vines CM, Wagener BM, Gurevich VV, Sklar LA, Prossnitz ER. Inhibition of chemoattractant N-formyl peptide receptor trafficking by active arrestins. *Traffic* 2005;**6**:87−99.
51. Rincon E, Rocha-Gregg BL, Collins SR. A map of gene expression in neutrophil-like cell lines. *BMC Genom* 2018;**19**:573.
52. Wilson B, Flett C, Gemperle J, Lawless C, Hartshorn M, Hinde E, et al. Proximity labelling identifies pro-migratory endocytic recycling cargo and machinery of the Rab4 and Rab11 families. *J Cell Sci* 2023; **136**:19.
53. Ren M, Xu G, Zeng J, De Lemos-Chiarandini C, Adesnik M, Sabatini DD. Hydrolysis of GTP on rab11 is required for the direct delivery of transferrin from the pericentriolar recycling compartment to the cell surface but not from sorting endosomes. *Proc Natl Acad Sci U S A* 1998;**95**:6187−92.
54. Li G, Marlin MC. Rab family of GTPases. *Methods Mol Biol* 2015; **1298**:1−15.
55. Homma Y, Hiragi S, Fukuda M. Rab family of small GTPases: an updated view on their regulation and functions. *FEBS J* 2021;**288**: 36−55.
56. Adler J, Parmryd I. Quantifying colocalization by correlation: the Pearson correlation coefficient is superior to the Mander's overlap coefficient. *Cytom Part A* 2010;**77a**:733−42.
57. Nagano M, Toshima JY, Siekhaus DE, Toshima J. Rab5-mediated endosome formation is regulated at the *trans*-Golgi network. *Commun Biol* 2019;**2**:419.
58. Amaya C, Militello RD, Calligaris SD, Colombo MI. Rab24 interacts with the Rab7/Rab interacting lysosomal protein complex to regulate endosomal degradation. *Traffic* 2016;**17**:1181−96.
59. Cheng XT, Xie YX, Zhou B, Huang N, Farfel-Becker T, Sheng ZH. Characterization of LAMP1-labeled nondegradative lysosomal and endocytic compartments in neurons. *J Cell Biol* 2018;**217**:3127−39.
60. Wang J, Ye RD. Agonist concentration-dependent changes in FPR1 conformation lead to biased signaling for selective activation of phagocyte functions. *Proc Natl Acad Sci U S A* 2022;**119**: e2201249119.
61. Grommes J, Soehnlein O. Contribution of neutrophils to acute lung injury. *Mol Med* 2011;**17**:293−307.
62. Ye RD, Boulay F, Wang JM, Dahlgren C, Gerard C, Parmentier M, et al. International union of basic and clinical pharmacology. LXXIII. Nomenclature for the formyl peptide receptor (FPR) family. *Pharmacol Rev* 2009;**61**:119−61.
63. Mehta D, Malik AB. Signaling mechanisms regulating endothelial permeability. *Physiol Rev* 2006;**86**:279−367.
64. Marasco WA, Phan SH, Krutzsch H, Showell HJ, Feltner DE, Nairn R, et al. Purification and identification of formyl-methionyl-leucyl-phenylalanine as the major peptide neutrophil chemotactic factor produced by *Escherichia coli*. *J Biol Chem* 1984;**259**:5430−9.
65. Abdullah N, Beg M, Soares D, Dittman JS, McGraw TE. Down-regulation of a GPCR by β-Arrestin2-mediated switch from an endosomal to a TGN recycling pathway. *Cell Rep* 2016;**17**:2966−78.
66. Tomas A, Vaughan SO, Burgoyne T, Sorkin A, Hartley JA, Hochhauser D, et al. WASH and Tsg101/ALIX-dependent diversion of stress-internalized EGFR from the canonical endocytic pathway. *Nat Commun* 2015;**6**:7324.
67. Mack M, Luckow B, Nelson PJ, Cihak J, Simmons G, Clapham PR, et al. Aminooxypentane-RANTES induces CCR5 internalization but inhibits recycling: a novel inhibitory mechanism of HIV infectivity. *J Exp Med* 1998;**187**:1215−24.
68. Marchese A, Paing MM, Temple BR, Trejo J. G protein-coupled receptor sorting to endosomes and lysosomes. *Annu Rev Pharmacol Toxicol* 2008;**48**:601−29.
69. Rajagopal S, Shenoy SK. GPCR desensitization: acute and prolonged phases. *Cell Signal* 2018;**41**:9−16.
70. Reiter E, Lefkowitz RJ. GRKs and beta-arrestins: roles in receptor silencing, trafficking and signaling. *Trends Endocrinol Metab* 2006; **17**:159−65.
71. Prossnitz ER, Kim CM, Benovic JL, Ye RD. Phosphorylation of the *N*-formyl peptide receptor carboxyl terminus by the G protein-coupled receptor kinase, GRK2. *J Biol Chem* 1995;**270**:1130−7.
72. Klaasse EC, Ijzerman AP, de Grip WJ, Beukers MW. Internalization and desensitization of adenosine receptors. *Purinergic Signal* 2008;**4**: 21−37.